analytical chemistry

Article

pubs.acs.org/ac

Sensitive Detection of Polycyclic Aromatic Molecules: Surface Enhanced Raman Scattering via $\pi-\pi$ Stacking

Yufeng Yuan,[†] Xiantong Yu,[†] Qiang Zhang,[‡] Mengfang Chang,[†] Lei Li,[†] Taiqun Yang,[†] Yuting Chen,[†] Haifeng Pan,[†] Sanjun Zhang,*[,†] Li Li,[§] and Jianhua Xu[†]

[†]State Key Laboratory of Precision Spectroscopy, [‡]Shanghai Key Laboratory of Regulatory Biology, School of Life Sciences, and [§]School of Chemistry and Molecular Engineering, East China Normal University, Shanghai, 200062, China

Supporting Information

ABSTRACT: We report silver nanoparticles (Ag NPs) with high stability, sensitivity, and no surface enhanced Raman scattering (SERS) background. The Ag NPs were synthesized via a one-step process with polysodium styrenesulfonate (PSSS) templates, and they could efficiently adsorb polycyclic aromatic molecules via $\pi-\pi$ stacking. The adsorption mechanisms and applicability were systematically studied by experimental measurements and theoretical simulations. When the polycyclic aromatic analytes were adsorbed on the PSSS-templated Ag NPs, the vibrations of $\pi-\pi$ stacking-bound moieties were attenuated, yet those of the other unbound aromatic moieties increased. Most importantly, when the analytes had more than two $\pi-\pi$ stacking binding sites, the PSSS-templated Ag NPs could trap the analytes by focusing through the optical force induced or via the simultaneously formed analyte−Ag NPs aggregates. This afforded high SERS intensity and very low detection limits.

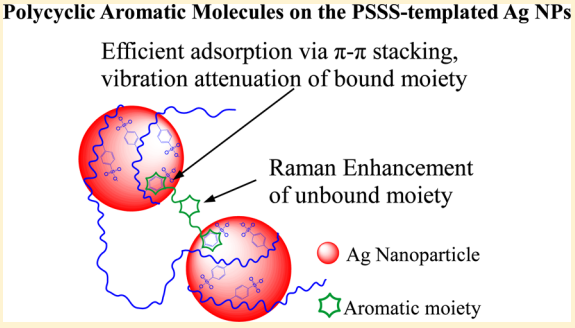

Polycyclic aromatic molecules are ubiquitous in natural substances. In life sciences, they are especially important for studying the structure and functions of enzymes/proteins, gene transcription, DNA repair, etc.[1−3] Sensitive detection and characterization of the polycyclic aromatic molecules is of great significance in biological redox processes such as metabolism, mitochondrial responses, immunological functions, cell survival, and apoptosis.[4−9] Various methods have been developed to explore aromatic molecules including high performance liquid chromatography (HPLC),[10] gas chromatography coupled to mass spectrometry,[11] capillary electrochromatography,[12] and enzyme assays.[4,5] However, most of these methods are time-consuming and require tedious sample preparation steps that may hamper their original properties, especially for molecules with biological activities.

Raman spectroscopy is useful in exploring the spectroscopic fingerprints of molecules, although the regular Raman scattering (RS) signal is very weak (about 14 orders of magnitude smaller than fluorescence).[13−15] Fortunately, this challenge has been improved via surface enhanced Raman scattering (SERS). SERS offers signal enhancements of 5−10 orders of magnitude when the analytes are adsorbed on the surface of metals (silver, gold, aluminum, copper, etc.).[13,16] Several adsorption mechanisms have been developed, and the interactions between analytes and SERS substrates play a key role in improving the efficiency of SERS. Analytes with cyanide (−CN) and thiol (−SH) can efficiently bind to the metal via covalent interactions,[17,18] while the noncovalent method is of particular interest because it can immobilize analytes on the surface with less distortion of the analyte molecules. Although the ionic analytes can be efficiently adsorbed on NPs modified with oppositely charged surfactant molecules, the surfactant usually induces SERS background. This may interfere with the SERS signals of analytes.[19] To overcome this shortcoming, charge-selective SERS substrates have been developed by depositing Ag and Au NPs on p- and n-type Si wafers or nanowires. This offers high selectivity for negatively and positively charged dyes, respectively.[20,21] Recently, the SERS detection of analytes with neither covalent nor charged binding groups, such as polycyclic aromatic hydrocarbons, has been reported via humic acid based silver nanoparticles (Ag NPs).[22] The adsorption mechanism was presumed to be $\pi-\pi$ stacking interactions. However, the complicated structure of humic acids resulted in SERS background noise. This limited the detection sensitivity to the range of tens of nM.[22]

Here, we designed Ag NPs for sensitive SERS detection and characterization of polycyclic aromatic molecules. The Ag NPs were synthesized in one step with polysodium styrenesulfonate (PSSS). They were found to efficiently adsorb aromatic analytes via the $\pi-\pi$ stacking interaction. Moreover, the influences of $\pi-\pi$ stacking adsorption on SERS characteristics and the applicability of analytes were systematically investigated.

Received: November 26, 2015
Accepted: March 25, 2016
Published: March 25, 2016

DOI: 10.1021/acs.analchem.5b04487
Anal. Chem. 2016, 88, 4328−4335

EXPERIMENTAL SECTION

Materials. All the reagents were used without any further purification. Flavin adenine dinucleotide disodium salt hydrate (FAD, 95%), rhodamine 6G, fluorescein, fluorescein sodium salt, poly sodium-4-styrenesulfonate (PSSS, MW: 1 000 000), pyridine (99.8%), and adenine (99%) were purchased from Sigma. Nicotinamide adenine dinucleotide disodium salt (NAD^+, 98%), its reduced form NADH (98%), and adenosine triphosphate (ATP, 98%) were purchased from Roche (Shanghai, China). The 2-phenylethanethiol (97%) and 1-pentanethiol (97%) were purchased from Tokyo Chemical Industry Co., Ltd. Silver nitrate ($AgNO_3$), sodium borohydride, trisodium citrate, nicotinamide, methylpyridine, 4,4′-bipyridine, absolute ethanol, iso-propanol, acetone, benzene, and methylbenzene were obtained from Sinopharm Chemical Reagent Co., Ltd. Ultrapure water with a resistivity of 18.2 MΩ·cm was used throughout.

Synthesis and Modification of Ag NPs. PSSS-templated Ag NPs were synthesized by reducing silver nitrate in one step at room temperature. Briefly, 250 μL (500 mg/L) of PSSS solution and 300 μL (10 mM) of freshly prepared sodium borohydride solution were mixed together with 5 mL (2.5 mM) of trisodium citrate solution. Next, 5 mL (0.5 mM) of silver nitrate solution was added into this reaction mixture solution at a certain rate (2.5 mL/min) under vigorous stirring. After the synthesis was complete, the color of the silver colloid was yellow. Bare Ag NPs were obtained according to the standard Creighton method with some modifications.[23] Briefly, 10 mL (1 mM) of silver nitrate solution and 30 mL (2 mM) of freshly prepared sodium borohydride solution were cooled for 20 min in an ice-bath. Next, 10 mL (1 mM) of silver nitrate solution was added dropwise into sodium borohydride solution with vigorous stirring in an ice-bath, and the colloid's color gradually became yellow. The freshly prepared bare Ag NPs were modified by mixing with 2-phenylethanethiol and 1-pentanethiol, respectively. The 2 mL of silver colloids were mixed with 100 μL (0.1 mM) of 2-phenylethanethiol (or 1-pentanethiol), and the mixed solutions were agitated for 10 s on a vortex shaker to produce efficient absorption. The modified Ag NPs were stored in the dark for UV−vis absorption and SERS measurements.

Characterization. The absorption spectral measurements were performed with a two-beam UV−vis spectrometer (TU-1901, Persee, China). The transmission electron microscopy (TEM) images of Ag NPs were taken using a HT 7700 system (Hitachi, Japan) at 100 kV. The samples (typically 10 μL) were added to the copper mesh and dried under clean conditions. To remove excessive reaction residues, the copper mesh was immersed in ultrapure water for 10 s. The samples were washed twice before TEM measurements. After, various analytes solutions were mixed and incubated with Ag NPs. The SERS spectra were obtained by a confocal Raman microscopy system (HORIBA Jobin Yvon T64000) equipped with a highly sensitive liquid-N_2-cooled charge-coupled detector. A 600 g/mm holographic grating blazed at 500 nm was used with a spectral resolution of 2 cm^{-1}.The excitation wavelength was 532 nm and was supplied with a single longitudinal solid laser (MSL-III-532 nm, line-width $<10^{-5}$ nm, CNI laser, China). The output power could reach 50 mW, but 500 μW was used for all samples. A band-pass interference filter (Semrock, LL01-532-25) was applied to prevent background emission from the laser source as well as a long pass Raman edge filter (Semrock, LP03-532RE-25) to eliminate the laser line. A water immersion microscope objective (Olympus, 60×, N.A = 1.2) was used for collection of the scattering signals. The Raman microscopy system was calibrated using the silicon line with the Raman band centered at 520 cm^{-1}. The original Raman spectra were preprocessed by LabSpec software. The correlated AFM and confocal Raman images were obtained with a scanning confocal microscope combined with an AFM (JPK NanoWizard II, Germany). The samples were focused under an oil-immersion microscope objective (Olympus, 100×, N.A = 1.40). The excitation beam was from a continuous-wave Nd:YAG laser, and the wavelength was 532 nm. A dichroic beam splitter and a 532 nm Raman long pass filter (Semrock, LP03−532RE-25) were used to remove excitation light. The SERS signals were detected with a single-photon counting module via a Si-avalanche photodiode (SPCM-AQR-14, PerkinElmer). The scanning areas of the AFM images were the same as those of the confocal Raman images. Both the AFM and confocal Raman images were analyzed and processed with Gwyddion software (Version 2.33). A batch of 2.2 × 2.2 cm glass slides were gradually and successively cleaned for 15 min with acetone, absolute ethanol, and iso-propanol in an ultrasonic bath. The glass slides were then immediately immersed into KOH (1 M) in ethanol solution for 15 min, rinsed with ultrapure water, and dried under nitrogen stream.[24] The treated slides were stored in a sealed container for atomic force microscopy (AFM). The PSSS-templated Ag NPs were mixed with the same volume of 1 fM FAD solution, and the mixture was vibrated for 20 s with a vortex shaker. To get efficient absorption, the FAD molecules were incubated for 2 h. Then, the mixture was diluted ten times with absolute ethanol, and 50 μL diluted solutions were deposited on the treated glass slides and allowed to dry for about 30 min under sealed conditions.

Simulation. We used density functional theory (DFT) to calculate the molecular Raman frequencies of NAD^+, NADH, fluorescein, fluorescein sodium, and FAD molecules. This was done in Gaussian 09 using a combination of the B3LYP hybrid exchange correlation function along with 6-31G+G (d, p) basis set. The geometry of the molecule was optimized prior to theoretical calculation. The $\pi-\pi$ stacking interactions were also performed with the Gaussian 09 package using the combination of the B3LYP hybrid exchange correlation function with 6-311++G (d, p) basis set. To estimate the amount of SERS enhancement factor from the electromagnetic enhancement, the local electromagnetic field distributions of Ag NPs and dimers were calculated by discrete dipole approximation (DDA).[25−28] The refractive index of silver at the excitation wavelength of 532 nm was obtained from the handbook.[29] We chose an array of closely spaced dipoles to replace a continuum target under the influence of the electric field of excitation light. The excitation light was a plane wave along the z-axis, and the electric field was polarized along the x-axis. To calculate the dimer, we assumed arraying along the x-axis such that the longitudinal modes were excited. The field enhancement can be investigated by calculating the ratio of the enhanced field to the incident field. The morphology of the dimer mimics the experimental results imaged by AFM. Computations were performed with DDSCAT 7.3 software.

RESULTS AND DISCUSSION

PSSS-templated Ag NPs were synthesized in one step by reducing silver nitrate with sodium borohydride in trisodium citrate and a PSSS mixture solution. Due to the strong

DOI: 10.1021/acs.analchem.5b04487
Anal. Chem. 2016, 88, 4328−4335

adsorption of PSSS-templated Ag NPs, the 500 nM flavin adenine dinucleotide (FAD) in water shows an intense SERS signal (Figure 1A, curve a). In contrast, the SERS signal of 500 nM FAD mixed with the bare Ag NPs (prepared by the well-known procedure[23]) was very weak (Figure 1A, curve b). Under the same experimental circumstances, the regular Raman scattering spectrum of FAD without any Ag NPs is barely detectable even at the highest concentration (100 mM; Figure 1A, curve c). Although the surfaces of Ag NPs were covered with PSSS, no remarkable Raman background was observed for PSSS-templated Ag NPs (Figure 1A, curve d). This has a superior advantage versus normal substrates with SERS background from the surfactants (Figure 2D).[22] Previous studies have shown that, when a single aromatic molecule is attached to the silver surface in parallel orientation, the in-plane vibrations of the aromatic ring can hardly be detected because the surface-enhanced field is normal to the surface and does not align with the transition dipole moments for the in-plane modes.[30,31] Therefore, our results imply that the benzene moiety of PSSS is parallel to the silver surface as illustrated in the inset of Figure 1B.

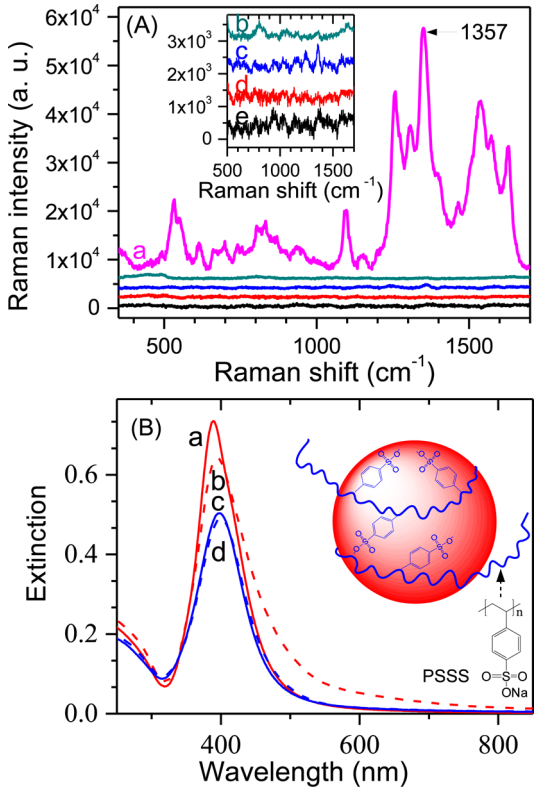

Figure 1. (A) The SERS spectra of 500 nM FAD with PSSS-templated Ag NPs (a) and bare Ag NPs (b), respectively. Curve (c) shows the regular Raman scattering spectrum of 100 mM FAD solution. Curves (d) and (e) show the SERS backgrounds of the PSSS-templated Ag NPs and bare Ag NPs, respectively. The inset displays the zoom of curves (b), (c), (d), and (e). The spectra are vertically displaced for clarity. The Raman peak at 1357 cm^{-1} is a distinct signature of FAD. The SERS spectra were recorded with a 532 nm laser, and the CCD integration time was normalized to 1 s. (B): The extinction spectra of freshly prepared bare Ag NPs (a), PSSS-templated Ag NPs (c), and their respective mixture with 500 nM FAD (curves b and d). The inset shows a schematic illustration of PSSS-templated Ag NPs and the chemical structure of PSSS. The TEM images of the PSSS-templated and bare Ag NPs are shown in Figure S1.

The intense SERS enhancement should be attributed to the strong interaction between FAD and the PSSS-templated Ag NPs. The adenine or flavin aromatic moieties of FAD could be adsorbed on the benzene moiety of PSSS through $\pi-\pi$ stacking interaction because the PSSS templates wrapped around the Ag NPs. This resulted in superior SERS signals. The $\pi-\pi$ stacking should be more efficient than the van der Waals force for the adsorption of polycyclic aromatic molecules (Figure 2). The Raman peak at 1357 cm^{-1} is a distinct signature of FAD and has a higher signal-to-noise ratio (SNR) for 2-phenylethanethiol-modified Ag NPs, which indicates that the efficiency of $\pi-\pi$ stacking is superior to the van der Waals force in polycyclic aromatic adsorption. Moreover, the 2-phenylethanethiol-modified Ag NPs had strong SERS background (curve a in Figure 2D). This may interfere with the SERS signal of polycyclic aromatic molecules.

The universality of PSSS-templated Ag NPs in SERS detection of polycyclic aromatic molecules has also been proven with the biological enzymes (NAD^+ and NADH) and optical dyes (fluorescein sodium and fluorescein) (Figure 3). Because of the similarity of their chemical structures, the limit of detection was 10 nM for both NAD^+ and NADH. It was 10 pM for both the fluorescein salt and fluorescein. With the help of density functional theory (DFT) simulations, the SERS bands at 740 cm^{-1} (range a) and 1000 cm^{-1} (range b) are related to the adenine and nicotinamide moieties of NAD^+/NADH, respectively. The main SERS bands at 1400 cm^{-1} (range c) manifest the overlapped vibrations of adenine and nicotinamide moieties (Figure 3A,B). As for the SERS spectra of fluorescein sodium and fluorescein (Figure 3C,D), the bands at 600 cm^{-1} (range a) are related to the hydroxyxanthen moiety, and the bands at 1400 cm^{-1} (range b) denote the overlapped vibrations of hydroxyxanthen and benzene carboxylate moieties. At high concentrations, the SERS spectra were similar to their respective DFT simulations. However, as the concentration of analytes decreased, the SERS spectra slightly changed and some bands disappeared. This indicates that the conformations or orientations of the analytes on PSSS-templated Ag NPs have changed. Of note, the SERS peaks at 1357 cm^{-1} could only be assigned to these analytes because DFT simulations and the regular Raman spectrum showed that PSSS does not have this peak (Figure S2). They are from the collective vibrations of the macromolecules. The low detection limits are comparable with conventional measurement methods such as fluorescence. The difference in detection limits between fluorescein sodium and NAD^+ is probably from their differences in Raman cross sections and adsorption efficiencies on the SERS substrates. In addition, the adsorption of these negative molecules (NADH and fluorescein sodium) on the PSSS-templated Ag NPs can not be attributed to electrostatic interactions because PSSS is a negative polymer. Thus, the similar low detection limits for the uncharged fluorescein and negatively charged fluorescein sodium confirmed that the PSSS-templated Ag NPs can efficiently adsorb polycyclic aromatic analytes via $\pi-\pi$ stacking. The PSSS-templated Ag NPs are candidate SERS substrates to study the properties of aromatic molecules such as the tryptophan−tryptophan dipeptide.[32]

Besides demonstration of the $\pi-\pi$ stacking in the efficient adsorption of polycyclic aromatic analytes, we further studied its influence on the Raman signal of analytes. When simple aromatic rings such as methylpyridine, pyridine, ATP,

DOI: 10.1021/acs.analchem.5b04487
Anal. Chem. 2016, 88, 4328−4335

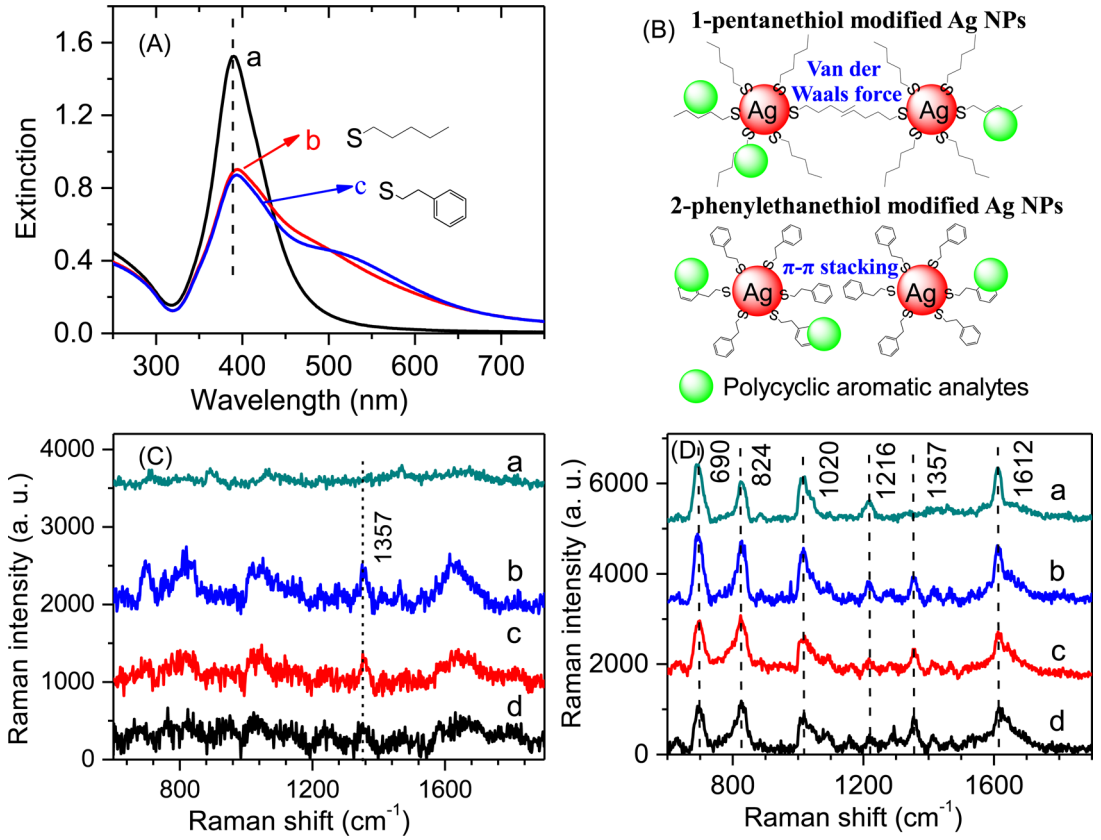

Figure 2. (A) The extinction spectra of freshly prepared Ag NPs (a) that were modified with 2.5 μM 1-pentanethiol-modified (b) or 2.5 μM 2-phenylethanethiol (c). (B) The schematic illustration of 1-pentanethiol and 2-phenylethanethiol-modified Ag NPs. The aggregation and affinity for polycyclic aromatic analytes of these two Ag NPs are presumed to be due to van der Waals forces and $\pi-\pi$ stacking, respectively. (C) (a) The SERS background of 1-pentanethiol-modified Ag NPs. The SERS spectra of FAD molecules with 50 nM (b), 500 nM (c), and 5 μM (d) concentrations mixed with 1-pentanethiol-modified Ag NPs. (D) (a) The SERS background of 2-phenylethanethiol-modified Ag NPs. The SERS spectra of FAD molecules with 50 nM (b), 500 nM (c), and 5 μM (d) concentration together with 2-phenylethanethiol-modified Ag NPs. The spectra in (C) and (D) are vertically displaced for clarity. The excitation laser wavelength was 532 nm, and the integration time was 30 s.

nicotinamide, or adenine were selected as the analytes, their SERS signals were barely detectable using PSSS-templated Ag NPs (Figure S3). Our results show that the SERS signals of 2-phenylethanethiol were decreased when we increased the FAD concentrations (peak at 690 cm^{-1} in Figure 2D). We propose that the vibration amplitude of interacting aromatic moieties may be dampened due to $\pi-\pi$ stacking, and both experimental and theoretical studies were performed to verify this proposal.

The SERS signal from the 10 mM pyridine was hardly detectable (Figure S3), but high intensity SERS signal was obtained for 100 μM 4,4-bipyridine (Figure 4A). DFT simulations show that the NRS band at 1001 cm^{-1} should be assigned to the breathing vibration of pyridine ring while the Raman bands at 1231, 1302, and 1620 cm^{-1} are attributed to collective stretch vibration of two pyridine rings. Of note, $\pi-\pi$ stacking between the pyridine ring and PSSS-templated Ag NPs results in a breathing vibration band at 1017 cm^{-1} that was significantly dampened in the SERS spectrum (curve b, Figure 4A). This was accompanied by the disappearance of a stretching vibration band (1231 cm^{-1}). A similar phenomenon was also observed for the biological coenzymes NAD^+/NADH in which two typical aromatic moieties, adenine and nicotinamide, are bridged together by a flexible pyrophosphate moiety. The SERS signal from the individual adenine and nicotinamide moieties were weak (Figure S3), but high intensity SERS signals were observed for the NAD^+/NADH (Figure 3A,B). Therefore, we propose that the $\pi-\pi$ stacking between PSSS-templated Ag NPs and analytes attenuates the vibration amplitude of adsorbed moieties. This results in extremely weak SERS signals for simple aromatic rings (methylpyridine, pyridine, ATP, nicotinamide, or adenine) on PSSS-templated Ag NPs. When polycyclic aromatic molecules with 2 $\pi-\pi$ stacking binding groups are adsorbed on the PSSS-templated Ag NPs, one aromatic moiety serves as the binding group and thus the vibrations are attenuated but with vibration enhancements from the other unbound aromatic moiety. Theoretical simulations were performed to verify this assumption. Aromatic interaction ($\pi-\pi$ stacking) can adopt different relative orientations, and these can be simply classified by three general cases: parallel-stacking, parallel-displaced, and edge-to-face.[33] In the parallel-stacking orientation, the surface contact is larger than those in the other cases. Thus, the interaction between the aromatic systems is at a maximum. In addition, the distance of $\pi-\pi$ stacking is 3.6–3.8 Å.[34] A simple $C_6F_6-C_6H_6$ dimer in the parallel-stacking model was adopted because characteristic breathing vibrations of C_6F_6 and C_6H_6 were located at 546 and 1007 cm^{-1}, respectively (Figure 4B). Simulation details are shown in the Supporting Information. Both the vibrations of C_6F_6 and C_6H_6 were attenuated when they were approached (Figure 4B). This shows that vibration attenuation is influenced by electronic and steric effects. The fact that the $\pi-\pi$ stacking interactions can attenuate the

DOI: 10.1021/acs.analchem.5b04487
Anal. Chem. 2016, 88, 4328–4335

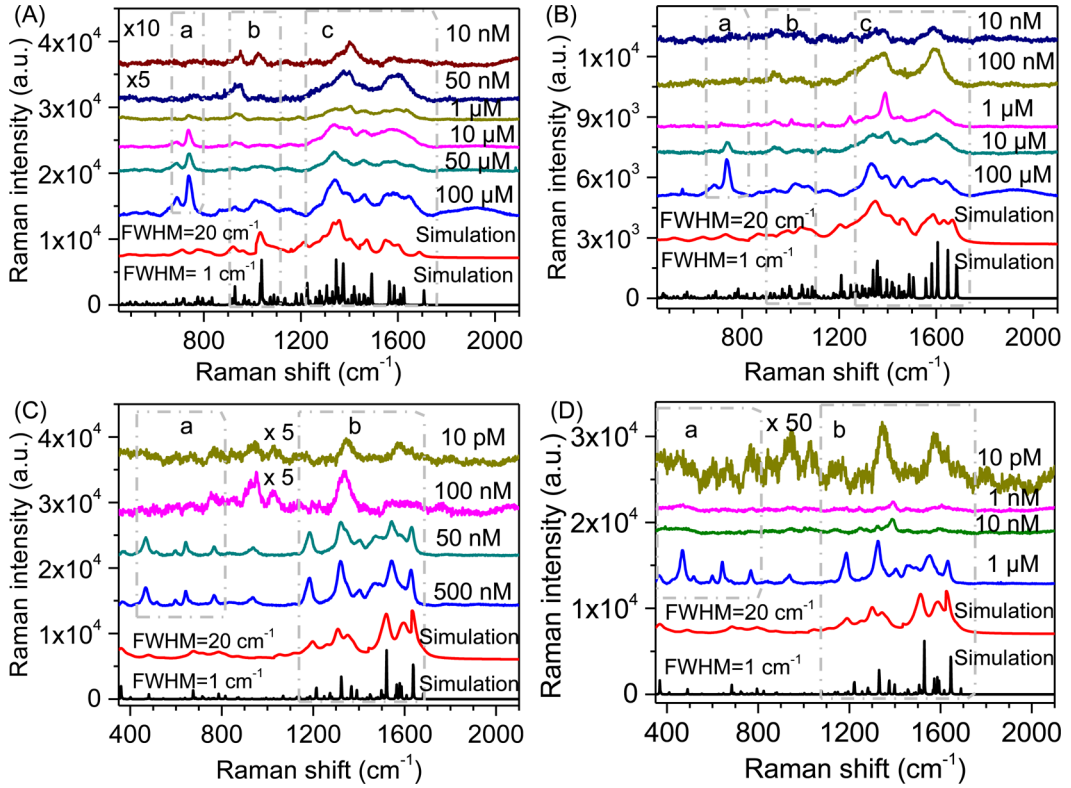

Figure 3. Simulated Raman spectra with various broadening (fwhm = 1 cm^{-1}, 20 cm^{-1}) and SERS spectra of NAD^+(A), NADH (B), fluorescein (C), and fluorescein sodium (D) at various concentrations based on PSSS-templated Ag NPs. The spectra in each panel are vertically displaced for clarity. The excitation laser wavelength was 532 nm, and the integration time of CCD was 1 s. The molecular Raman vibrations were calculated by DFT.

vibration amplitude of aromatic molecules has been observed but not clearly interpreted. Some Raman peaks were weakened or even disappeared when carbon nanotubes were assembled with terphenyl or pyrene via $\pi-\pi$ stacking.[35,36] Therefore, the PSSS-templated Ag NPs are only suggested in the SERS detection of polycyclic aromatic molecules with at least 2 $\pi-\pi$ stacking binding groups.

Besides demonstrating that the SERS characteristics of PSSS-templated Ag NPs are dependent on the type of aromatic molecules, we further studied its dependence on analyte concentrations. Figure 5 presents a series of SERS spectra measured at FAD concentrations from 50 μM to 5 aM at 10-fold steps. The SERS signals were intense and reproducible at high FAD concentrations and were weaker as a function of FAD concentrations. However, when FAD concentrations were further decreased, the SERS signals became lower but statistically detectable until very low concentrations (<fM). However, the probability of detection continued to decrease. The relationship between SERS intensities and FAD concentrations clearly show two phases corresponding to high (Phase I) and low (Phase II) FAD concentrations (Figure 5B). Time-dependent absorption and SERS spectra were measured to study the interactions between PSSS-templated Ag NCs and FAD at various concentrations (Figures 6, S4, and S5). The high FAD concentrations (5 μM) caused the PSSS-templated Ag NCs to aggregate, and their absorption peaks red-shifted by 24 nm in 140 h (Figure S4A).

However, lower FAD concentrations could not cause the PSSS-templated Ag NCs to aggregate because both the absorption peaks red-shifted by 8 nm in 140 h for FAD concentrations of 500 nM and 500 fM (Figure S4B,C). This is identical to that without FAD (Figure S4D). Continuous SERS spectra were captured every 10 s after the PSSS-templated Ag NPs, and 500 nM FAD solutions were mixed and incubated for various times (15 min, 45 min, 550 min, and 20 h in Figures 6A and S5). The SERS signals were always weak at the beginning and became stronger with increased measurement time. The excitation laser beam created a gradient force trap at the focus of the objective lens. This induced the PSSS-templated Ag NPs and FAD aggregate (Figure 5; phase I). The TEM images show that the diameter of PSSS-templated Ag NPs are smaller than 30 nm; these are usually impossible to be trapped at the focus because the optical force scales with the volume of trapped object. However, these Ag NPs are linked by PSSS chains, which increased the effective volume and held them in focus. Moreover, the aggregation process can bring the adjacent PSSS-templated Ag NPs and FAD molecules into focus to make the local concentration inside the focus much higher than in solution. The SERS intensity became stable and reproducible after a certain measurement time (~100 s) at high FAD concentrations (Figures 6A and S5). Thus, at high FAD concentrations (Phase I), although the FAD molecules have already been adsorbed on the surface of PSSS-templated Ag NPs, the aggregations that afford high SERS signals were formed very quickly (~100 s). This was only after the excitation optical field was applied.

For the PSSS-templated Ag NCs and 500 aM FAD solution (Phase II), the SERS signals can be observed with low probability only when FAD molecules happened to be located at the focus. Once the FAD molecules were in the focus, the SERS signals were rather stable during the measurement time (Figure 6B). This indicates that no more neighboring FAD molecules were further trapped at the focus because of the low FAD concentrations. As a consequence, the average FAD

DOI: 10.1021/acs.analchem.5b04487
Anal. Chem. 2016, 88, 4328−4335

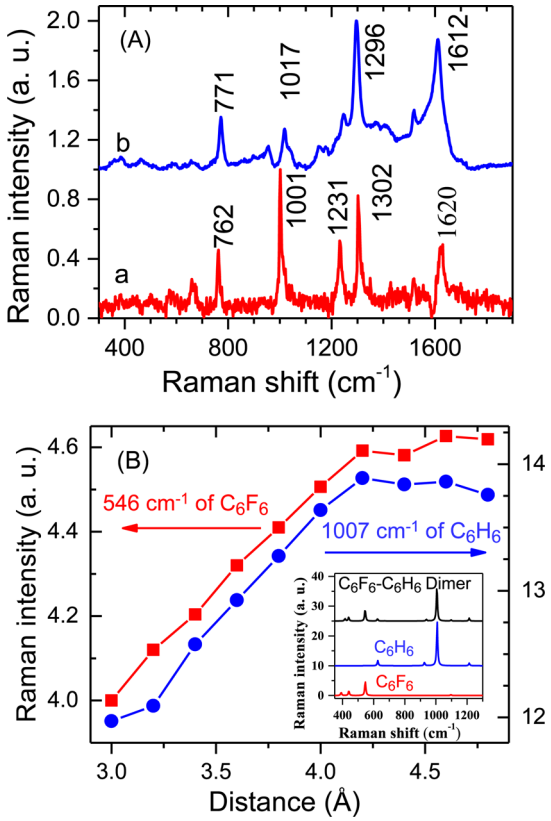

Figure 4. (A) (a) The regular Raman scattering spectrum of 4,4-bipyridine powder. (b) SERS spectrum of 100 μM 4,4-bipyridine based on PSSS-templated Ag NPs. The incident laser wavelength was 532 nm. Integral time was normalized to 1 s. (B) The Raman intensities of C_6F_6 (546 cm^{-1}) and C_6H_6 (1007 cm^{-1}) vs the distance between the C_6F_6–C_6H_6 dimer in parallel-stacking model. The inset displays the simulated Raman spectra of C_6F_6, C_6H_6, and C_6F_6–C_6H_6 dimer, respectively. The spectra are vertically displaced for clarity.

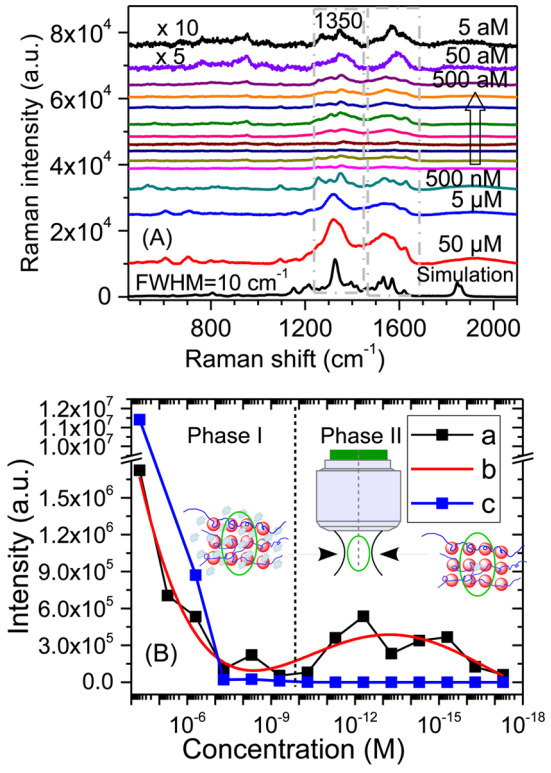

Figure 5. (A) The SERS spectra of FAD molecules obtained at various concentrations. The spectra are vertically displaced for clarity. The FAD concentrations were from 50 μM to 5 aM with a step of 10-fold. (B) The comparison of the SERS intensities of FAD molecules on PSSS-templated Ag NPs (curve a) and fluorescence intensities of R6G (curve c) in various concentrations. Curve b is the polyfit of curve a. The measurements were performed under the same experimental circumstances with incident laser wavelength of 532 nm and integration time of 1 s. The intensities were obtained by integrating from 540 to 600 nm for the fluorescence of R6G and in 1320–1440 cm^{-1} for the SERS of FAD.

concentration shown in Figure 6 does not correspond to the local FAD concentration in focus. It only indicates that the FAD was highly diluted. As a direct comparison, the SERS intensities of the FAD became much higher than the fluorescence intensities of Rhodamine 6G (R6G) at low concentrations (Figure 5B).

The PSSS-templated Ag NPs enhanced the SERS intensity of FAD at very low concentrations (Phase II) probably due to two mechanisms. First, the FAD adsorbed on PSSS-template Ag NPs may be trapped at the focus during the measurement time; otherwise, the FAD molecules can only stay at the focus for a very short time due to Brownian motion. Second, the SERS spectra were stable from the very beginning of the measurement time; this suggests that the SERS signals came from structures completely formed prior to measurement. FAD has two π–π stacking binding moieties (adenine and flavin). Thus, it is possible that a portion of FAD molecules can bridge two PSSS-templated Ag NPs to simultaneously form dimer or multimer assemblies. This could significantly enhance the near-field electromagnetic field in the gap due to their interference.[37−39] The FAD-bridged dimer/multimer assemblies guarantee that the FAD molecules can be located in the gap (hotspots). The FAD-bridged dimer/multimer assemblies could afford very high SERS signals because the SERS intensity is proportional to the fourth power of the local field.[40,41] This structure should be formed very slowly due to self-assembly under the circumstance that the surfaces of most Ag NPs have adequate available binding sites. The formation of these aggregates can not be monitored by absorption spectroscopy due to their low proportions.

Correlated AFM and Raman imaging was employed to screen the SERS in ultralow analyte concentration (Phase II). In the solution of 500 aM, the FAD and PSSS-templated Ag NPs were dispersed on the substrate, and the SERS signals were mainly from beads in thread-like structures; these are the PSSS-templated Ag NPs and FAD assemblies (Figure S6). After 100-fold dilution and substrate dispersion of the 500 aM FAD and PSSS-templated Ag NPs, the dimer/multimer assemblies were clearly visualized by AFM (Figure S7A). A discrete dipole approximation (DDA) simulation was performed to confirm the near-field enhancement for the dimer configuration. When the Ag NPs form a dimer, the electrical field enhancement factor (E/E_0) could be increased from 4.65 to 140 for the horizontal polarization (Figure S7C,D). This corresponds to a SERS intensity enhancement of ~7 orders of magnitude. Thus, we propose that the SERS of FAD could be observed at very low concentrations perhaps due to the simultaneously formed dimer/multimer assemblies.

DOI: 10.1021/acs.analchem.5b04487
Anal. Chem. 2016, 88, 4328−4335

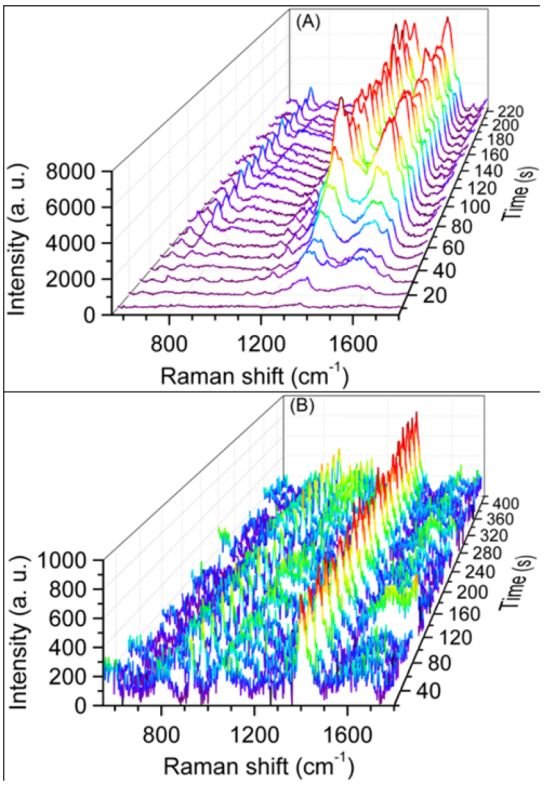

Figure 6. (A) Time-dependent SERS spectra for 500 nM FAD and PSSS-templated Ag NPs solution after an incubation time of 15 min. The same characterization was performed for longer incubation times (45 min, 550 min, and 20 h; Figure S5). (B) Time-dependent SERS spectra captured in the 500 aM FAD and PSSS-templated Ag NPs solution after an incubation time of 30 min. The SERS signals were excited with a 532 nm laser and a 60× water immersion microscope objective.

CONCLUSION

In conclusion, we designed and synthesized PSSS-templated Ag NPs for the sensitive SERS detection of polycyclic aromatic molecules. The PSSS-templated Ag NPs exhibited high stability, no SERS background noise, and high sensitivity. The adsorption mechanism and applicability of analytes were exhaustively studied via experimental measurements (including Raman spectroscopy, UV−vis absorption, transmission electron microscopy, correlated atomic force microscopy, and confocal Raman imaging) as well as theoretical simulations (density functional theory and discrete dipole approximation). The benzene moieties of PSSS could adsorb the polycyclic aromatic analytes via $\pi-\pi$ stacking, which has been confirmed by the high sensitive detections of FAD, NAD^+/NADH, fluorescein/fluorescein sodium, etc. If the analytes have only one $\pi-\pi$ stacking binding site (methylpyridine, pyridine, ATP, nicotinamide, or adenine), then the vibrations of analytes were attenuated after being adsorbed on the PSSS-templated Ag NPs. In contrast, when the analytes have two $\pi-\pi$ stacking binding sites (such as 4,4-bipyridine, NAD^+/NADH, etc.), the vibrations of the bound moiety are attenuated but the Raman signals of the other unbound moiety are enhanced after the analytes are adsorbed on the PSSS-templated Ag NPs. Most importantly, when the analytes have more than two $\pi-\pi$ stacking binding sites and their chemical structures meet certain requirements, such as structure flexibility and steric encumbrance, the PSSS-templated Ag NPs could help trap the analytes at the focus through optical force induced or simultaneously formed analytes/Ag NPs aggregates. This offered high SERS intensity and very low detection limits. Fortunately, these requirements could be easily satisfied in some polycyclic aromatic macromolecules including enzymes, DNA, and proteins. The Ag NPs may offer highly sensitive SERS characterization to these molecules with wide potential application. Moreover, our study paves the way for designing new SERS sensors for some typical polycyclic aromatic molecules.

ASSOCIATED CONTENT

Supporting Information

The Supporting Information is available free of charge on the ACS Publications website at DOI: 10.1021/acs.analchem.5b04487.

TEM images, SERS spectra, time-resolved extinction and SERS spectra, and correlated confocal and Raman imaging, Supplementary Figures S1−S7. (PDF)

AUTHOR INFORMATION

Corresponding Author

*Tel.:+86 21 6223 5573. E-mail: sjzhang@phy.ecnu.edu.cn.

Notes

The authors declare no competing financial interest.

ACKNOWLEDGMENTS

The authors thank professors Yang Tian, E Wu, Xiao He, John Z. H. Zhang, and Ms. Min Song for their assistance in experiments and simulations. This work was partly supported by the National Science Foundation of China (61178085, 6141001145, 61008003), the Science and Technology Commission of Shanghai Municipality (15520711500, 15ZR1411700), and the Program of Introducing Talents of Discipline to Universities (B12024).

REFERENCES

(1) Feng, L.; Gell, D. A.; Zhou, S. P.; Gu, L. C.; Kong, Y.; Li, J. Q.; Hu, M.; Yan, N.; Lee, C.; Rich, A. M.; Armstrong, R. S.; Lay, P. A.; Gow, A. J.; Weiss, M. J.; Mackay, J. P.; Shi, Y. G. *Cell* **2004**, *119*, 629−640.
(2) Yu, J.; Xiao, J.; Ren, X. J.; Lao, K. Q.; Xie, X. S. *Science* **2006**, *311*, 1600−1603.
(3) Saltiel, A. R.; Kahn, C. R. *Nature* **2001**, *414*, 799−806.
(4) Zhang, Q. H.; Wang, S. Y.; Nottke, A. C.; Rocheleau, J. V.; Piston, D. W.; Goodman, R. H. *Proc. Natl. Acad. Sci. U. S. A.* **2006**, *103*, 9029−9033.
(5) Zhang, Q. H.; Piston, D. W.; Goodman, R. H. *Science* **2002**, *295*, 1895−1897.
(6) Yang, H. Y.; Yang, T.; Baur, J. A.; Perez, E.; Matsui, T.; Carmona, J. J.; Lamming, D. W.; Souza-Pinto, N. C.; Bohr, V. A.; Rosenzweig, A.; de Cabo, R.; Sauve, A. A.; Sinclair, D. A. *Cell* **2007**, *130*, 1095−1107.
(7) Vemuri, G. N.; Eiteman, M. A.; McEwen, J. E.; Olsson, L.; Nielsen, J. *Proc. Natl. Acad. Sci. U. S. A.* **2007**, *104*, 2402−2407.
(8) Skala, M. C.; Riching, K. M.; Gendron-Fitzpatrick, A.; Eickhoff, J.; Eliceiri, K. W.; White, J. G.; Ramanujam, N. *Proc. Natl. Acad. Sci. U. S. A.* **2007**, *104*, 19494−19499.
(9) Lin, S. J.; Guarente, L. *Curr. Opin. Cell Biol.* **2003**, *15*, 241−246.
(10) Dost, K.; Ideli, C. *Food Chem.* **2012**, *133*, 193−199.
(11) Tseng, W. C.; Chen, P. S.; Huang, S. D. *Talanta* **2014**, *120*, 425−432.
(12) Xie, W. J.; Xu, A. S.; Yeung, E. S. *Anal. Chem.* **2009**, *81*, 1280−1284.

DOI: 10.1021/acs.analchem.5b04487
Anal. Chem. 2016, 88, 4328−4335

(13) Pieczonka, N. P. W.; Aroca, R. F. *Chem. Soc. Rev.* **2008**, *37*, 946−954.
(14) Nie, S. M.; Emery, S. R. *Science* **1997**, *275*, 1102−1106.
(15) Kneipp, J.; Kneipp, H.; Kneipp, K. *Chem. Soc. Rev.* **2008**, *37*, 1052−1060.
(16) Yguerabide, J.; Yguerabide, E. E. *Anal. Biochem.* **1998**, *262*, 137−156.
(17) Freeman, R. G.; Grabar, K. C.; Allison, K. J.; Bright, R. M.; Davis, J. A.; Guthrie, A. P.; Hommer, M. B.; Jackson, M. A.; Smith, P. C.; Walter, D. G.; Natan, M. J. *Science* **1995**, *267*, 1629−1632.
(18) Laurentius, L.; Stoyanov, S. R.; Gusarov, S.; Kovalenko, A.; Du, R. B.; Lopinski, G. P.; McDermott, M. T. *ACS Nano* **2011**, *5*, 4219−4227.
(19) Kumar, A.; Joshi, H.; Pasricha, R.; Mandale, A. B.; Sastry, M. *J. Colloid Interface Sci.* **2003**, *264*, 396−401.
(20) Baik, S. Y.; Cho, Y. J.; Lim, Y. R.; Im, H. S.; Jang, D. M.; Myung, Y.; Park, J.; Kang, H. S. *ACS Nano* **2012**, *6*, 2459−2470.
(21) Bhatt, K.; Tan, S.; Karumuri, S.; Kalkan, A. K. *Nano Lett.* **2010**, *10*, 3880−3887.
(22) Qu, L. L.; Li, Y. T.; Li, D. W.; Xue, J. Q.; Fossey, J. S.; Long, Y. T. *Analyst* **2013**, *138*, 1523−1528.
(23) Creighton, J. A.; Blatchford, C. G.; Albrecht, M. G. *J. Chem. Soc., Faraday Trans. 2* **1979**, *75*, 790−798.
(24) Zhang, S. J.; Audebert, P.; Wei, Y.; Al Choueiry, A.; Lanty, G.; Brehier, A.; Galmiche, L.; Clavier, G.; Boissiere, C.; Lauret, J. S.; Deleporte, E. *Materials* **2010**, *3*, 3385−3406.
(25) Sow, I.; Grand, J.; Levi, G.; Aubard, J.; Felidj, N.; Tinguely, J. C.; Hohenau, A.; Krenn, J. R. *J. Phys. Chem. C* **2013**, *117*, 25650−25658.
(26) Mahmoud, M. A. *Langmuir* **2013**, *29*, 6253−6261.
(27) Draine, B. T.; Flatau, P. J. *J. Opt. Soc. Am. A* **2008**, *25*, 2693−2703.
(28) Smith, D. A.; Stokes, K. L. *Opt. Express* **2006**, *14*, 5746−5754.
(29) Palik, E. D. *Handbook of Optical Constants of Solids*; Academic Press: San Diego, 1998.
(30) Moskovits, M. *J. Chem. Phys.* **1982**, *77*, 4408−4416.
(31) Moskovits, M.; Suh, J. S. *J. Phys. Chem.* **1984**, *88*, 5526−5530.
(32) Yuan, Y.; Qu, J.; Song, J.; Xiong, M.; Liu, J. *Opt. Mater. Express* **2016**, *6*, 146−154.
(33) Hunter, C. A.; Sanders, J. K. M. *J. Am. Chem. Soc.* **1990**, *112*, 5525−5534.
(34) Cozzi, F.; Annunziata, R.; Benaglia, M.; Baldridge, K. K.; Aguirre, G.; Estrada, J.; Sritana-Anant, Y.; Siegel, J. S. *Phys. Chem. Chem. Phys.* **2008**, *10*, 2686−2694.
(35) Zhang, Y.; Yuan, S. L.; Zhou, W. W.; Xu, J. J.; Li, Y. *J. Nanosci. Nanotechnol.* **2007**, *7*, 2366−2375.
(36) Gregan, E.; Keogh, S. M.; Maguire, A.; Hedderman, T. G.; Neill, L. O.; Chambers, G.; Byrne, H. J. *Carbon* **2004**, *42*, 1031−1035.
(37) Dadosh, T.; Sperling, J.; Bryant, G. W.; Breslow, R.; Shegai, T.; Dyshel, M.; Haran, G.; Bar-Joseph, I. *ACS Nano* **2009**, *3*, 1988−1994.
(38) Michaels, A. M.; Jiang, J.; Brus, L. *J. Phys. Chem. B* **2000**, *104*, 11965−11971.
(39) Elezgaray, J.; Berguiga, L.; Argoul, F. *Appl. Phys. Lett.* **2010**, *97*, 97.
(40) GarciaVidal, F. J.; Pendry, J. B. *Phys. Rev. Lett.* **1996**, *77*, 1163−1166.
(41) Le Ru, E. C.; Etchegoin, P. G. *Principles of Surface-Enhanced Raman Spectroscopy*; Elsevier: Amsterdam, 2009.

DOI: 10.1021/acs.analchem.5b04487
Anal. Chem. 2016, 88, 4328−4335